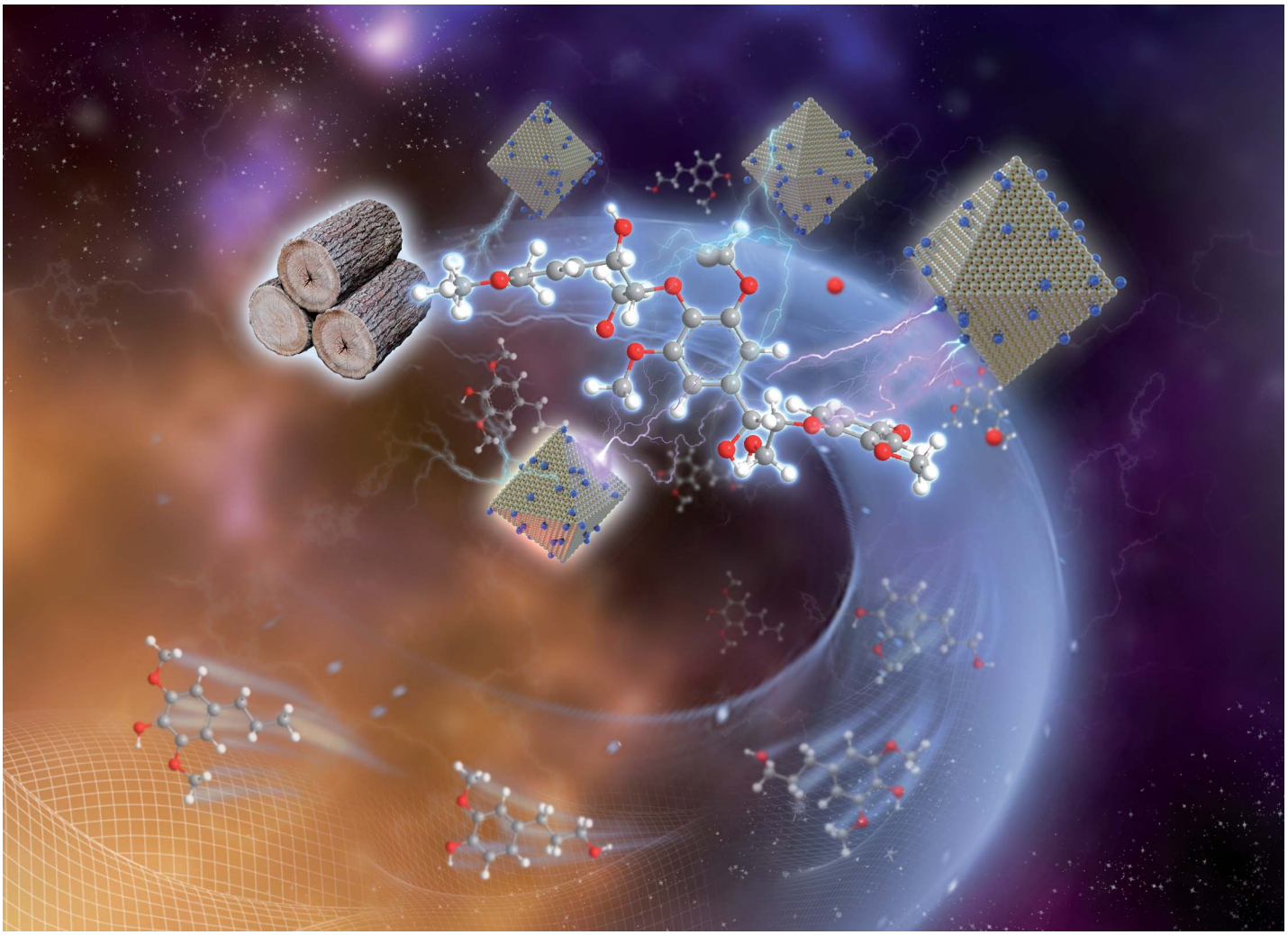

Showcasing research from Professor Run-Cang Sun and Ling-Ping Xiao's laboratory, Liaoning Key Lab of Lignocellulose Chemistry and BioMaterials, College of Light Industry and Chemical Engineering, Dalian Polytechnic University, Dalian, China.

Metal–organic framework-derived CuO catalysts for the efficient hydrogenolysis of hardwood lignin into phenolic monomers

This work reports a metal-organic framework (MOF) derived copper oxide catalyst (CuO/c-UiO-66), which exhibits superior catalytic properties toward the reductive catalytic deconstruction of hardwood lignin into monomeric phenols with a high yield up to 42.8 wt%. The synergistic effects of the fabricated catalyst and hydrogen facilitate the efficient C–O bond scission of the methoxylated β-*O*-4′ intermediates.

As featured in:

See Ling-Ping Xiao, Run-Cang Sun *et al.*, *J. Mater. Chem. A*, 2023, **11**, 23809.

ROYAL SOCIETY OF CHEMISTRY

rsc.li/materials-a

Registered charity number: 207890

Journal of Materials Chemistry A

ROYAL SOCIETY OF CHEMISTRY

PAPER

View Article Online
View Journal | View Issue

Cite this: J. Mater. Chem. A, 2023, 11, 23809

Metal–organic framework-derived CuO catalysts for the efficient hydrogenolysis of hardwood lignin into phenolic monomers†

Qian Xu, Qiang Wang, Ling-Ping Xiao, * Xiao-Ying Li, Xi Xiao, Meng-Xin Li, Meng-Ran Lin, Yu-Man Zhao and Run-Cang Sun *

Received 17th August 2023
Accepted 22nd October 2023

DOI: 10.1039/d3ta04927b

rsc.li/materials-a

The selective reductive catalytic deconstruction (RCD) of lignin into phenolic monomers provides the possibility for making the full use of lignocellulose. However, the widespread use of precious metal catalysts and the harsh reaction conditions present the challenge of poor industrial utilization in the current research. Herein, we report a metal–organic framework (MOF)-derived copper oxide catalyst (CuO/c-UiO-66), which exhibits superior catalytic properties in the RCD of hardwood lignin and affords high yields (up to 42.8 wt%) of monomeric phenols *via* the C–O bond scission. The mechanistic reactions using lignin model compounds reveal that phenolic compounds with propyl or propanol end chains are selectively produced during the catalytic hydrogenolysis reaction. The enhanced catalytic reactivity is attributed to the synergy of acid and base sites of the catalyst, which facilitates the C–O bond cleavage process. The new insights of this study provide guidance toward the rational design of Cu-based catalysts for RCD of lignin.

1. Introduction

Lignocellulose is a nonedible biomass feedstock, which is made up of cellulose (30–50%), hemicellulose (20–35%), and lignin (15–30%).[1] In particular, lignin is a heterogeneous biomacromolecule, representing the largest and most widely renewable carbon resource.[2,3] Such sustainable carbon feedstock can be used as an alternative to produce bio-fuels and bio-based materials.[4,5] Currently, to relieve the fossil energy crisis, increasing attention has been put into the efficient utilization of lignocellulose materials to replace petroleum-derived chemicals with sustainable alternatives.[6,7] Phenolic monomers from lignin depolymerization serve as an upstream product of aromatic chemicals.[8–11] However, the natural complexity and heterogeneity of lignin restrain its efficient utilization.[12] Additionally, the lignin undergoes structural rearrangement during the isolation or pulping process and forms irreversible C–C bonds while sacrificing the tenuous β-*O*-4′ linkages, thus resulting in the difficult transformation of industrial lignin.[13] Therefore, the recalcitrant lignin in the papermaking industry is always burned as fuel to provide the energy needed for the pulp industry.[14,15] In spite of extensive efforts, the efficient transformation of lignin into valuable chemicals is still challenging.[15–17]

Many efficient strategies have been explored for lignin depolymerization. Reductive catalytic deconstruction (RCD) is an effective method to produce aromatic platform chemicals from lignin.[18–22] This strategy enables the efficient hydrogenolysis of lignin to phenolic compounds without affecting the chemical carbohydrate's structural integrity for further processing.[20,23] The hydrogen-donor suitable solvents, degree of reaction, and catalysts could increase the product yield in RCD.[21,24,25] Lower-grade aliphatic alcohols, which have hydrogen donor characteristics, are often applied as organic solvents as they not only increase dissolution at the depolymerization interface and prevent char formation but also offer *in situ* hydrogen resources during the hydrogenolysis process of lignin.[26] Moreover, they behaved differently as hydrogen donors during the hydrogenolysis of lignocellulose owing to their different reactivity.[27] For example, Kim and co-workers[28] reported that the more polar alcohols seemed to be much effective in inhibiting the repolymerization process during the catalytic hydrogenolysis of biomass.

The fundamental challenge of RCD of woody sawdust is the selective dissociation of aryl-ether linkages while preserving aromaticity, which requires tailored catalysts. In this process, many precious metal catalysts, such as Ru[3,29,30] and Pd,[31,32] have been reported to produce monomeric phenols with end chains by cleaving the C–O linkage from β-*O*-4′ lignin units. Sels' group[33] used a commercial Ru/C catalyst for the hydrogenolysis of birch wood and obtained 50.5 wt% phenolic compounds,

Liaoning Key Lab of Lignocellulose Chemistry and BioMaterials, Liaoning Collaborative Innovation Center for Lignocellulosic Biorefinery, College of Light Industry and Chemical Engineering, Dalian Polytechnic University, Dalian 116034, China. E-mail: lpxiao@dlpu.edu.cn; rsun3@dlpu.edu.cn

† Electronic supplementary information (ESI) available. See DOI: https://doi.org/10.1039/d3ta04927b

wherein guaiacol and syringol with propyl side chains were the major monomers. Huang and co-workers[34] disclosed that 55 wt% mono-aromatics could be obtained from native birch lignin with small amounts of Pd/C. Hu *et al.*[35] revealed that the bimetallic catalyst (Ni–Pd) was more active during the hydrogenolysis of birch native lignin than the parent monometallic catalysts, which was due to the 'synergistic effects'.[36–38] However, the capability of the bimetallic catalysts for hydrogenolysis of native lignin is still unclear.[17] Moreover, precious metal catalysts show limitations in large-scale industrial applications due to their scarcity and high price. Therefore, a number of researchers have taken note of the development of non-precious metal catalysts. For example, MoO_x/SBA-15 showed high selectivity to produce monolignols and etherized derivatives in the hydrogenolysis of woody biomass.[39] Rautiainen and co-workers[40] reported that the Co-based catalyst could effectively break down the β-*O*-4′ bonds of birch lignin, affording the yield of aromatic monomers up to 34 wt%. For lignin hydrogenolysis, catalysts based on copper have been rarely investigated. Ford and co-workers[41,42] described a Cu-doped porous metal oxide-based catalyst for lignin decomposition to cyclohexyl derivatives by hydrogenolysis of phenyl ether bonds in super-critical methanol. Hensen *et al.*[43] presented a $CuMgAlO_x$ catalyst for catalytic degradation of alkaline lignin in ethanol, which resulted in 23 wt% monomer yield. The Cu_{20}PMO catalyst has been used for the hydrogenolysis of aryl-ether linkages, which was effective for C–O bond scission.[44]

Metal–organic frameworks (MOFs) have attracted great interest owing to their chemical tenability, large surface area, high catalytic activity, pore structure, and abundant metal sites.[45–48] The framework can limit tiny metal nanoparticles within either holes/cages or crystalline defects, thus creating a metal–support surface for catalysis. Recently, Song's group[23] reported selective production of phenolic compounds under different reaction conditions from *Eucalyptus* lignin with a Ni@ZIF-8 catalyst. Notably, the active metal centers and abundant metal sites of MOFs prompted our enthusiasm for developing active catalysts with a MOF-analogue structure.[49] We are also concerned with recent advances in the study of MOF-derived catalysts, where the active metal center is anchored to the derivatized framework, forming catalyst structural sites that exhibit excellent catalytic performance for catalysis.[50,51] Zr-based MOFs are widely used in catalysis due to their unique high specific surface area and tunable crystal structure.[52–55] We conjectured that UiO-66 containing Zr atoms might regulate the selectivity control in RCD of lignocellulosic biomass. Herein, we report that CuO supported on a UiO-66 derived framework (CuO/collapse-UiO-66, abbreviated as CuO/c-UiO-66) acts as a highly efficient catalyst for the RCD of the native lignin in hardwood lignocellulosic biomass. Moreover, we have improved the performance of Cu-based catalysts in terms of stability as compared to previously reported catalysts (CuO/C) with the same CuO active site.[56] In addition, this catalytic system could obtain a range of phenolic compounds in high yields by switching reaction conditions. Finally, the behavior of lignin model compounds over CuO/c-UiO-66 was also investigated to verify the reaction mechanism in this work.

2. Experimental section

2.1 Preparation of the catalyst

2.1.1 Synthesis of UiO-66. UiO-66 was prepared by a hydrothermal synthesis procedure with a minor modification according to a previous report.[57] Concisely, 0.9342 g of $ZrCl_4$ and 0.6651 g of H_2BDC were dissolved in 80 mL *N*,*N*-dimethylformamide (DMF) with ultrasound for 20 min. The obtained mixture was subsequently transferred to a reactor and placed under heat at 120 °C for 24 h. A white powder was obtained by centrifugation, washed several times with methanol and then put in an oven overnight at 60 °C.

2.1.2 Synthesis of CuO/collapse-UiO-66 (CuO/c-UiO-66). 0.2508 g UiO-66 was added to 50 mL of methanol with sonication for 30 min. Subsequently, 0.2397 g $CuAc_2 \cdot H_2O$ was mixed with the above suspension, followed by 1 h of magnetic stirring at room temperature. After that, a fresh $NaBH_4$/MeOH solution (1.45 mg mL^{-1}) was immediately mixed with the aforementioned dispersion and mechanically stirred for 2.5 h. The precipitate was gathered by filtration and washed with methanol, and after that dried at 60 °C for 12 h. Finally, the product was calcinated in air at 400 °C for 2 h, which was designated as CuO/collapse-UiO-66 (CuO/c-UiO-66) (Fig. 1a).

2.2 General process for RCD of native lignin from lignocellulose

Overall, wood sawdust (50 mg), CuO/c-UiO-66 (20 mg) and a polar solvent (10 mL) were loaded into a 50 mL stainless steel batch reactor (Parr Instruments Co.), which was then sealed and purged with N_2 and then pressurized with H_2 (3 MPa) at room temperature. The reaction was carried out at different temperatures for a certain time. At the end of the reaction, the reactor was cooled to room temperature and carefully depressurized. The resulting mixture of reacted insoluble solids was then filtered by solid–liquid separation and washed several times with dichloromethane (DCM) to ensure maximum retention of the lignin depolymerization products. Subsequently, the solution fractions were extracted with DCM. After removal of all volatiles under vacuum, the resulting oil was quantitatively and qualitatively analyzed using gas chromatography (GC) and gas chromatography-mass spectrometry (GC-MS), respectively.

2.3 Reusability of the CuO/c-UiO-66 catalyst

At the end of the hydrogenolysis process, the catalyst and carbohydrate fractions were left as insoluble fractions. In order to carry out the recycling performance test, we had to isolate the used catalyst. By blocking the carbohydrate fraction using a 200 mesh (0.074 mm) sieve, the small-sized catalyst escaped through the pores. Finally, the spent CuO/c-UiO-66 catalyst was used for the next run.

2.4 General characterization

Surface areas were calculated from the adsorption data using Brunauer–Emmett–Teller (Beijing Builder Co. Ltd, China). Samples were allowed to degas under vacuum prior to

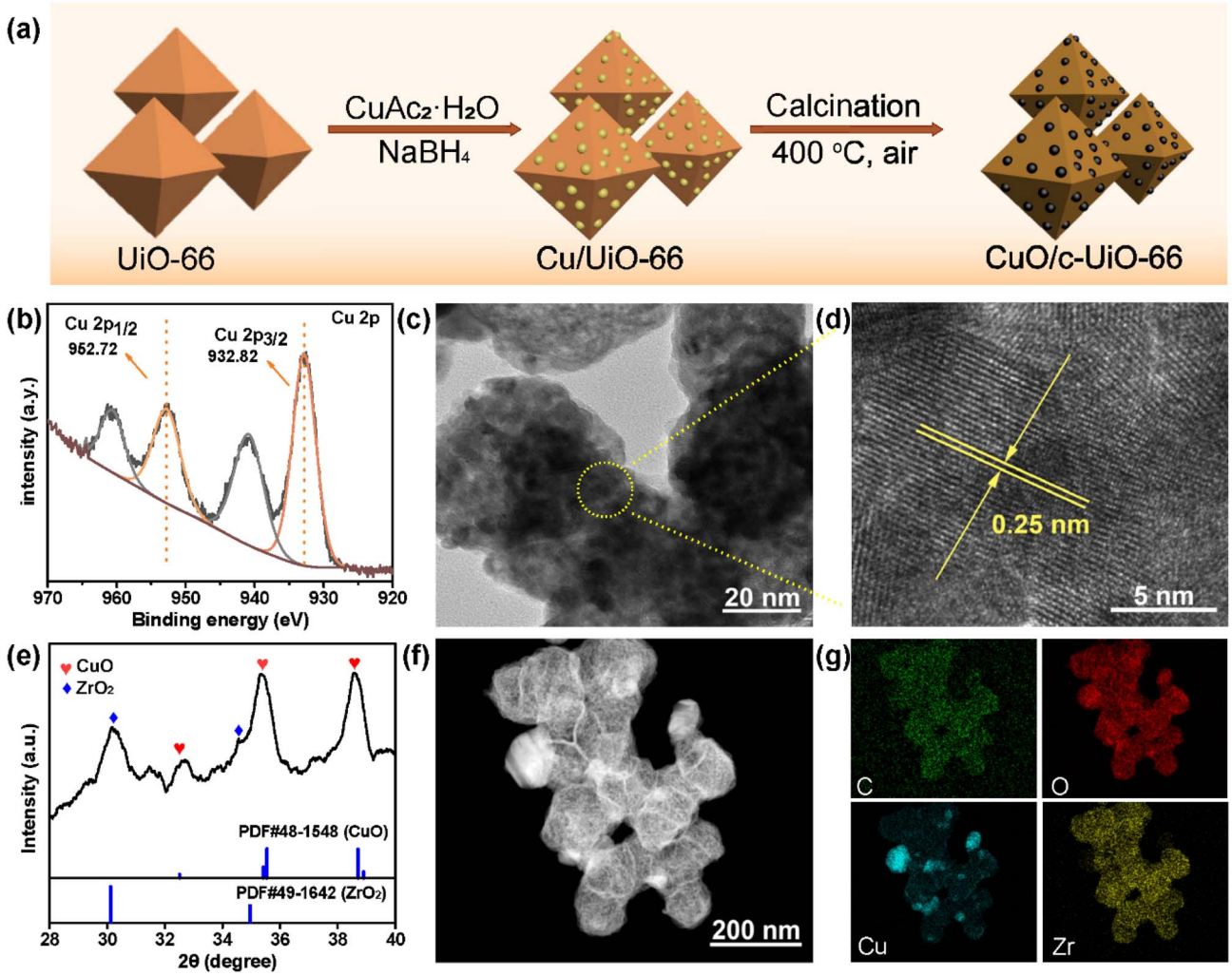

Fig. 1 (a) Diagram of the preparation of CuO/c-UiO-66; morphology and structure characterization of CuO/c-UiO-66: (b) XRD patterns; (c) and (d) high resolution TEM images; (e) XPS spectrum of Cu 2p; and (f) and (g) HR-STEM image and corresponding EDX elemental mapping of C, O, Cu and Zr.

measurement for 5 h at 300 °C. X-ray diffraction (XRD) analysis was performed on a Shimadzu Lab XRD-6100 diffractometer with a Cu Kα radiation source operating at 15 mA with 40 kV. X-ray photoelectron spectra (XPS) were obtained using a scanning X-ray microprobe (PHI 5000 Versa, ULAC-PHI, Inc.) with AI Kα emission and 284.80 eV C 1s peak used as an internal standard. After catalyst samples were dissolved in hydrogen fluoride (HF) solution, the Cu and Zr content was measured through inductively coupled plasma atomic emission spectroscopy (ICP-AES) using a Thermos IRIS Intrepid II XSP emission spectrometer. Transmission electron microscopy (TEM) was performed using a JEM-2100F FETEM fitted with an energy dispersive X-ray spectrometer (EDX) for analysis at 100 kV, and a high-angle annular dark-field scanning TEM (HAADF-STEM). EDX elemental mapping was carried out at 200 kV. The NH_3-TPD was tested on Micromeritics AutoChem II 2920 apparatus to determine the number of acid sites. Typically, about 100 mg of the catalyst was restored in the H_2 stream at 200 °C for 1 h, and before being cooled down to room temperature in the He stream. NH_3-TPD was allowed to increase at temperatures from 50 °C to 650 °C at 10 °C min^{-1} for 30 min. CO_2-TPD assays were performed on Micromeritics Autochem 2920 apparatus. A sample was restored at 300 °C, then purged for 1 h with a 10% H_2/Ar stream, and chilled to 50 °C in a He flow. After being exposed to a 5% CO_2/He flow (1 h; 50 °C) and purged with He (1 h; 50 °C), the sample was treated to 500 °C at 5 °C min^{-1} in a 30 cm per min He stream, and the dehydrogenated gas was examined by TCD.

Molecular weight distributions of lignins and oily products were determined by gel permeation chromatography (GPC) utilizing a Waters 1515 isocratic pump equipped with a Dual Absorbance UV detector (Waters 2487) set at 280 nm with an Agilent Plgel 3 μm 100 Å 300 × 7.5 mm column as described previously.[58] Notably, the lignin samples were firstly acetylated and then dissolved in THF (2 mg mL^{-1}) and finally purified through a 0.45 μm syringe filter before injection.[59]

Gas chromatography (GC) and gas chromatography-mass spectrometry (GC-MS) analyses were performed on

a Shimadzu Model 2010 plus with an HP-5 column (30 m × 0.25 mm × 0.25 mm) employing a flame ionization detector (FID) and a Shimadzu GCMS-QP2010SE with an HP-5MS (30 m × 0.25 mm × 0.25 mm) column, respectively. Injection temperature was 250 °C. The column temperature was heated from 50 °C and held for 3 min, then ramped at 8 °C min^{-1} to 280 °C, and held for 5 min at that temperature. The injection temperature of the FID was 200 °C. The characterization and quantification of lignin monomers within oil-based products have been performed by reference to real samples obtained from commercial sourcing or independent synthesis. The monomer yields were calculated using the formula

$$\text{Monomer yield (wt\%)} = \frac{\text{mass(monomer)}}{\text{mass(initial lignin)}} \times 100\% \quad (1)$$

$$\text{Monomer yield (\%)} = \frac{\text{mole(monomer)}}{\text{mole(lignin mimics)}} \times 100\% \quad (2)$$

Nuclear magnetic resonance (NMR) spectra were obtained on a Bruker Ascend-400 MHz spectrometer.[56] Samples of lignin (~60 mg) were added to 0.55 mL of DMSO-d_6 and 0.14 mL of pyridine, and then ultrasonicated until the solids dissolved. Samples of lignin oil (~60 mg) were solubilized in DMSO-d_6. As for two-dimensional heteronuclear single-quantum correlation (2D HSQC) NMR, the solvent peak (DMSO-d_6) at δ_C/δ_H 39.5/2.49 ppm was used as an internal reference.

3. Results and discussion

3.1 Catalyst characterization

The preparation of CuO/c-UiO-66 is schematically illustrated in Fig. 1a. Clearly, the XRD pattern of crystalline phases of CuO/c-UiO-66 indicated that the CuO was dispersed on the framework of UiO-66 (Fig. 1b). The fabricated CuO/c-UiO-66 catalyst displayed typical peaks at 2θ of 32.5°, 35.5° and 38.7° indexed to (110), (11−1) and (111), respectively, which are attributed to CuO (PDF #48-1548). The pattern also showed the (111) and (200) diffractions of ZrO_2 at 30.1° and 35.0°, respectively (PDF #49-1642). This revealed that the active species in the catalyst was CuO, which was in agreement with the +2 state of oxidation of Cu in CuO with the following XPS results. Notably, the Cu 2p spectrum in Fig. 1e revealed two signals at 932.82 eV and 952.72 eV, which are allotted to Cu $2p_{3/2}$ and Cu $2p_{1/2}$ corresponding to the data of CuO,[60] respectively. In addition, the TEM images indicated a lattice spacing identified as 0.25 nm, which conformed to the (11−1) plane of CuO nanocrystallites (Fig. 1c and d). This result was consistent with the XRD pattern. The HAADF-STEM of CuO/c-UiO-66 suggested that CuO nanoparticles were dispersed on the Zr-based carrier framework (Fig. 1f).

Catalysts with both acid–base and metal sites exhibit excellent catalytic activity for the RCD of lignin. Generally, NH_3-TPD of CuO/c-UiO-66 showed two peaks, suggesting the presence of weak and medium acidic sites (Fig. 2a). The desorption peak at ~275 °C was due to the result of NH_3 adsorbed on Lewis acid sites.[61] The acid site of CuO/c-UiO-66 promoted lignin depolymerization without significantly causing the recombination of lignin reaction intermediates. The surface alkalinity of CuO/c-UiO-66 was investigated by CO_2-TPD (Fig. 2b), and peaks situated at low temperature ranging from 120 to 200 °C are ascribed to carbon species adsorbed to weakly basic sites, which are due to hydroxyl groups at the metal oxide surface (CuO).[18] The desorption of CO_2 resulted in strongly basic sites at high temperatures, which are attributed to coordinatively unsaturated O^{2-} ions.[62] The metal site has the capacity to break the ether bond and the base site has the ability to assist in hydrogenation. Moreover, it was observed that the specific surface area (69.1 m^2 g^{-1}) of CuO/c-UiO-66 decreased after the immobilization of copper on UiO-66 (294.7 m^2 g^{-1}). UiO-66 displayed a significantly higher specific surface area, which might benefit active site dispersion. On the side, the porous structure of UiO-66 confined the metal pellet effectively, forming smaller CuO particles and thus offering more active sites for RCD of lignin.

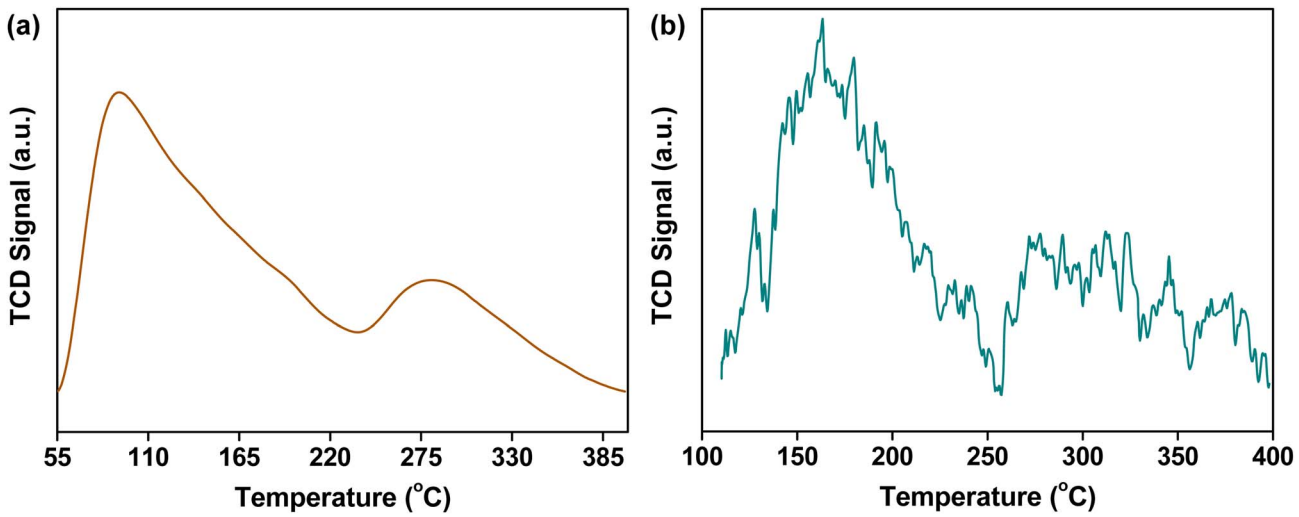

Fig. 2 (a) NH_3-TPD profile of CuO/c-UiO-66; (b) CO_2-TPD profile of CuO/c-UiO-66.

The percentage by weight of elemental Cu in CuO/c-UiO-66 was determined to be 39.9% according to ICP-AES (Table S1†).

3.2 Catalytic hydrogenolysis of poplar sawdust

Poplar sawdust was chosen for probing the potential of CuO/c-UiO-66 for the catalytic hydrogenolysis in the lignin-first system. Firstly, we analyzed the chemical composition of poplar wood. It was found that this hardwood consisted of 24.9 wt% lignin (22.4 wt% of Klason lignin and 2.5 wt% acid-soluble lignin), 42.7 wt% cellulose, and 19.7 wt% hemicellulose (Table S5†).

Then, the treatment of poplar sawdust with 20 mg CuO/c-UiO-66 under 3 MPa H_2 at 240 °C in MeOH for 2 h afforded a soluble fraction with lignin oily products and an insoluble fraction with carbohydrate slurry as well as the catalyst. To identify and quantify the lignin-derived products, the lignin oily product was subjected to comparative analysis with GC by comparison with respective real samples. Clearly, it was found that 4-*n*-propanolsyringol (**S1**, 14.7 wt%), 4-*n*-propylsyringol (**S2**, 9.9 wt%), 4-*n*-propanolguaiacol (**G1**, 5.6 wt%) and 4-*n*-propylguaiacol (**G2**, 3.0 wt%) were the main monophenols, which are dependent on the total amount of lignin in the feedstock (Fig. 3a). As a contrast, a control experiment without the catalyst at 240 °C involving heating the poplar sawdust for 2 h was given, which resulted in a dark lignin oil with only 6.7 wt% total monomers (Table S7†). The average molecular weight (M_w) of the lignin oil (475 g mol^{-1}) was sharply decreased as compared to that of DEL isolated from poplar (10 850 g mol^{-1}) as determined by GPC (Fig. 3b). With the purpose of proving the CuO importance in the catalytic hydrogenolysis system, we used d-

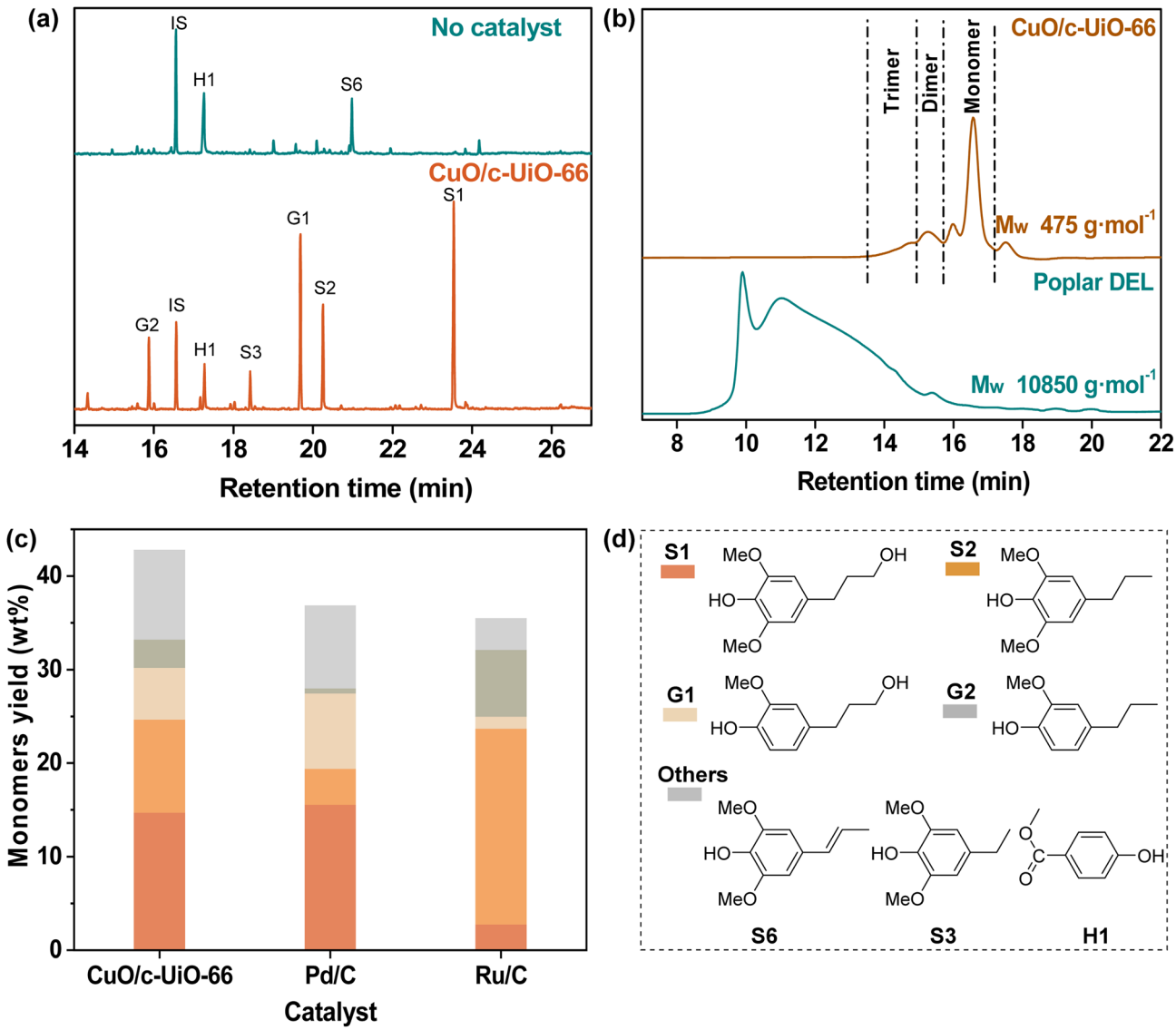

Fig. 3 (a) GC of lignin oil obtained from the catalytic hydrogenolysis of poplar sawdust with or without the CuO/c-UiO-66 catalyst; (b) GPC analysis of double enzymatic lignin (DEL) and lignin oil obtained by RCD of poplar sawdust over the CuO/c-UiO-66 catalyst. (c) Comparison of the monomeric yields obtained from RCD of poplar sawdust over the CuO/c-UiO-66 with those of commercial catalysts of Pd/C and Ru/C. (d) Structures of monomers. Reaction conditions: poplar sawdust (50 mg), catalyst (20 mg), MeOH (10 mL), H_2 (3 MPa), 240 °C, and 2 h.

UiO-66 (the framework would decompose when the UiO-66 was calcined alone at 400 °C, so we denoted it as decompose-UiO-66, abbreviated as d-UiO-66) instead of CuO/c-UiO-66 at 240 °C for 2 h with 3 MPa H_2 in MeOH (Fig. S9†). The obtained high content of dimethyl terephthalate indicated that the UiO-66 derived framework was broken down under the hydrogenolysis reaction conditions. This result suggested that CuO was indispensable in the hydrogenolysis reaction. Additionally, we used the CuO catalyst and ZrO_2 catalyst in the reaction (Fig. S9†). It was found that the CuO catalyst alone was active in the hydrogenolysis reaction of poplar lignin, but was less selective for the propanol group and the propanol side chain products. The ZrO_2 catalyst was inactive in this reaction. We speculated that CuO was the main active substance in this reaction system, and the MOF-derived framework as a support might assist in modulating the selectivity of copper oxide and further improve the catalytic activity.

In general, the precious metals Pd and Ru have excellent effects on catalytic hydrogen hydrolysis. So, a control experiment with commercially available catalysts, Pd/C and Ru/C, was performed for comparison under the conditions of 240 °C at MeOH for 2 h (Fig. 3c), which afforded relatively lower monomer yields than CuO/c-UiO-66 of 36.9 wt% and 35.4 wt%, respectively (Table S9†). Notably, the fabricated CuO/c-UiO-66 exhibits comparable hydrogenolysis activity toward RCD of lignin into monophenols with those of state-of-the-art catalysts (Table S16†).[39,40,63–67]

These results suggested that the fabricated CuO/c-UiO-66 nanomaterial was an efficient catalyst toward the RCD of lignin into monophenols in high yields. Moreover, it was observed that monophenols with less preservation of γ-OH over the Ru/C catalyst were obtained, which could be ascribed that less hydrogenation epimer of Ru/C than CuO/c-UiO-66 gave a chance for priority hydrogenolysis.[68]

The aromatic and side chain regions of poplar DEL and lignin oily product of 2D HSQC NMR spectra are illustrated in Fig. 4, demonstrating the sufficient scission of lignin C–O bonds and product distributions after the RCD process. Notably, in the aromatic area, a significant reduction in signals was observed for **G2**, $G_{5,6}$, and $S_{2,6}$ (Fig. 4b). Moreover, in the side chain region, the detected cross-peaks of 4-propylphenols **S/G1** are identified at δ_C/δ_H 31.7/2.50, 34.8/1.70 and 61.0/3.43 ppm (labeled in orange), and the signals at δ_C/δ_H 37.9/2.44, 24.8/1.55, and 14.1/0.87 ppm are ascribed to the propanol chain ascribed to **S/G2** (labeled in blue) (Fig. 4b). Furthermore, no signal was detected for β-*O*-4′, demonstrating the active dissociation of lignin over the CuO/c-UiO-66 catalyst. This result revealed that nearly all the aryl-ether linkages in poplar lignin have been decomposed by C–O bond cleavage under the hydrogenolysis reaction conditions.

3.3 Investigation of reaction conditions

In order to further understand the behavior of CuO/c-UiO-66, a series of experiments were undertaken, which aimed to further explore the optimal reaction conditions. Hydrogen might assist CuO/c-UiO-66 to resist the tendency of lignin recondensation reactions,[63] so we kept the condition of 3 MPa H_2 unchanged. First of all, we have designed catalysts with different Cu doping percentages for the hydrogenolysis of lignin, and the catalytic effect was relatively best when the molar ratio of Cu/Zr was 1.2 (Table S7†). Then, we explored the influence of different catalyst dosages (Fig. 5a), and the highest monomeric yield was obtained when the catalyst dosage was 20 mg. Different solvents were selected in the RCD of poplar sawdust over CuO/c-UiO-66, such as MeOH, EtOH, ^{i}PrOH, and dioxane (Fig. 5b). The CuO/c-UiO-66 catalyst showed maximum activity in MeOH toward the hydrogenolysis of poplar lignin under 240 °C for 4 h. The soluble fraction extracted by CH_2Cl_2 gave the oil-like product with an overall aromatic monomer yield of 42.9 wt%, from which **S1** and **S2** were in the highest yield. GPC analysis was applied to further examine the allocation of oligomers, dimers, and monomers in the lignin oil. A sharp decrease in M_w was observed from the 10 850 g mol^{-1} of DEL as compared to the 470 g mol^{-1} of oily products (Fig. S18†). Similarly, both EtOH and ^{i}PrOH as the hydrogen donating solvents in the process showed reduced overall yields in comparison with that from MeOH in obtaining the phenolic monomers, while the high selectivity for **S1** remained. This was in good agreement with the prior reports that the **S** unit always showed high reactivity in hydrogenolysis of lignin over late-transition-metal catalysts.[69,70] Moreover, an increase of M_w was observed in the hydrogenolysis solvents EtOH (620 g mol^{-1}) and ^{i}PrOH (1060 g mol^{-1}) as compared to that of MeOH (470 g mol^{-1}). This could be explained that the greater the polarity of the alcohol, the greater the hydrogen supply capacity and the more favorable to the RCD of lignin. However, in the case of ^{i}PrOH, an array of monomeric phenols with unsaturated substituents were formed in 15.0 wt% yield (Table S11†). This result might be due to the poor lignin solubility in ^{i}PrOH during this depolymerization process, thus resulting in the ether linkages among lignin units not being sufficiently fragmented.[71] Moreover, the catalytic properties of the CuO/c-UiO-66 for RCD of lignin in dioxane were significantly reduced with a sharp drop in total monomer yield (25.0 wt%). This result was consistent with previous reports that alcohols performed better in the hydrogenolysis of lignin due to their superior hydrogen-donating ability.[72]

Further optimization of the reaction temperature in RCD of poplar sawdust with the CuO/c-UiO-66 catalyst has also been investigated (Fig. 5c). It was observed that raising the temperature to 260 °C, the hydrogenolysis reaction produced a lower total yield of monomers (32.9 wt%) and higher M_w values (550 g mol^{-1}) as compared with those at 240 °C (42.9 wt%; 470 g mol^{-1}) (Table S12 and Fig. S20†). These results are probably due to satisfactory cleavage of the majority of the C–O linkages and the retention of C–C bonds at such a temperature. Lowering the reaction temperature (~200 and 220 °C) below 240 °C resulted in no loss of selectivity, but it led to a reduction in yield of 33.3 wt% and 40.3 wt%, respectively. The possible reason for these results was incomplete cleavage of ether bonds between lignin units due to insufficient temperature.

The influence of different reaction times on CuO/c-UiO-66-catalyzed hydrogenolysis of lignin was subsequently explored

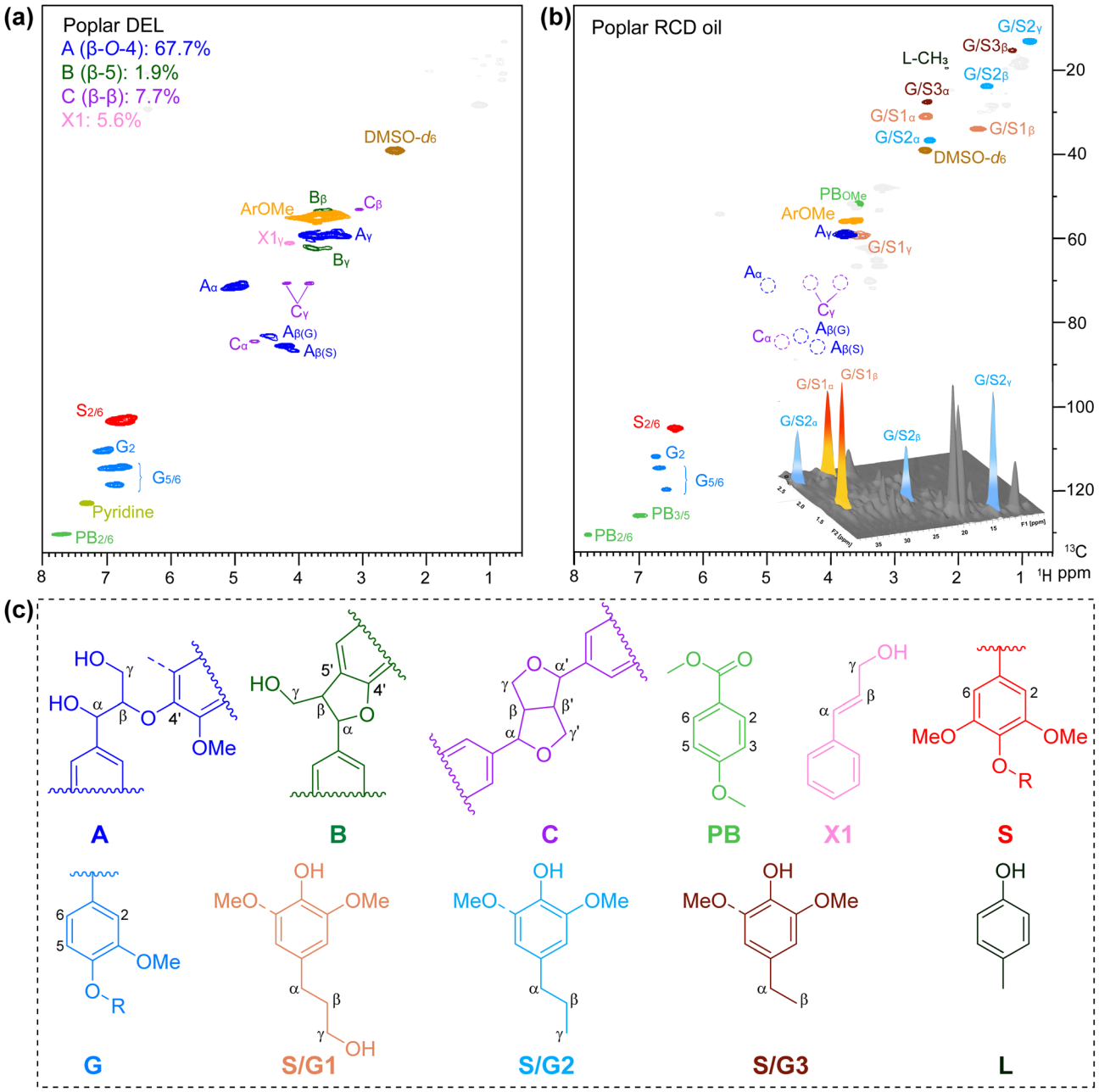

Fig. 4 2D HSQC NMR spectrum of (a) DEL isolated from poplar and (b) lignin oily products from RCD of poplar over the CuO/c-UiO-66 catalyst. (c) Primary structure exhibited in the 2D HSQC NMR spectra: (**A**) β-*O*-4′ alkyl–aryl ether, (**B**) β-5′ phenylcoumaran, (**C**) β-β′ resinol, (**PB**) *p*-hydroxybenzoates, (**X1**) cinnamyl alcohol end-groups, (**S**) syringyl units, (**G**) guaiacyl units, (**S1**) 4-*n*-propanolsyringol, (**S2**) 4-*n*-propylsyringol, (**G1**) 4-*n*-propanolguaiacol, (**G2**) 4-*n*-propylguaiacol, (**S3**) 2,6-dimethoxy-4-ethylphenol, (**G3**) 4-ethylguaiacol, and (**L**) 4-methyl phenol. Reaction conditions: poplar sawdust (50 mg), CuO/c-UiO-66 catalyst (20 mg, 39.9 wt%), MeOH (10 mL), H_2 (3 MPa), 240 °C for 4 h.

(Fig. 5d). Remarkably, 28.8 wt% monomeric phenols could be obtained at 0.5 h (Table S13†), which demonstrated the efficient catalytic activity of CuO/c-UiO-66. When prolonging the time to 1 h, a lignin oil with a monophenol yield of 37.2 wt% and M_w of 540 g mol^{-1} was generated. Although shorter times were also effective for the hydrogenolysis of lignin, the shortage of time might lead to insufficient exposure between the active site of CuO/c-UiO-66 and lignin, which resulted in an inadequate catalytic effect. Accordingly, the reaction times were suitably extended and the total aromatic monomer yield was stable after 2 h. That is to say, the use of a range of reaction times indicated that 2 h was sufficient for the C–O bond scissions. In summary, the favorable conditions for RCD of poplar sawdust over the CuO/c-UiO-66 catalyst in MeOH could efficiently convert lignin biopolymers to phenolic monomers with a relatively high yield (up to 42.8 wt%) and lowest M_w (475 g mol^{-1}) with 3 MPa H_2 at 240 °C for 2 h.

The ability to recover the catalyst was subsequently discussed. At the end of the hydrogenolysis process, a 200 mesh (0.074 mm) screen was used to effectively allow the small sized

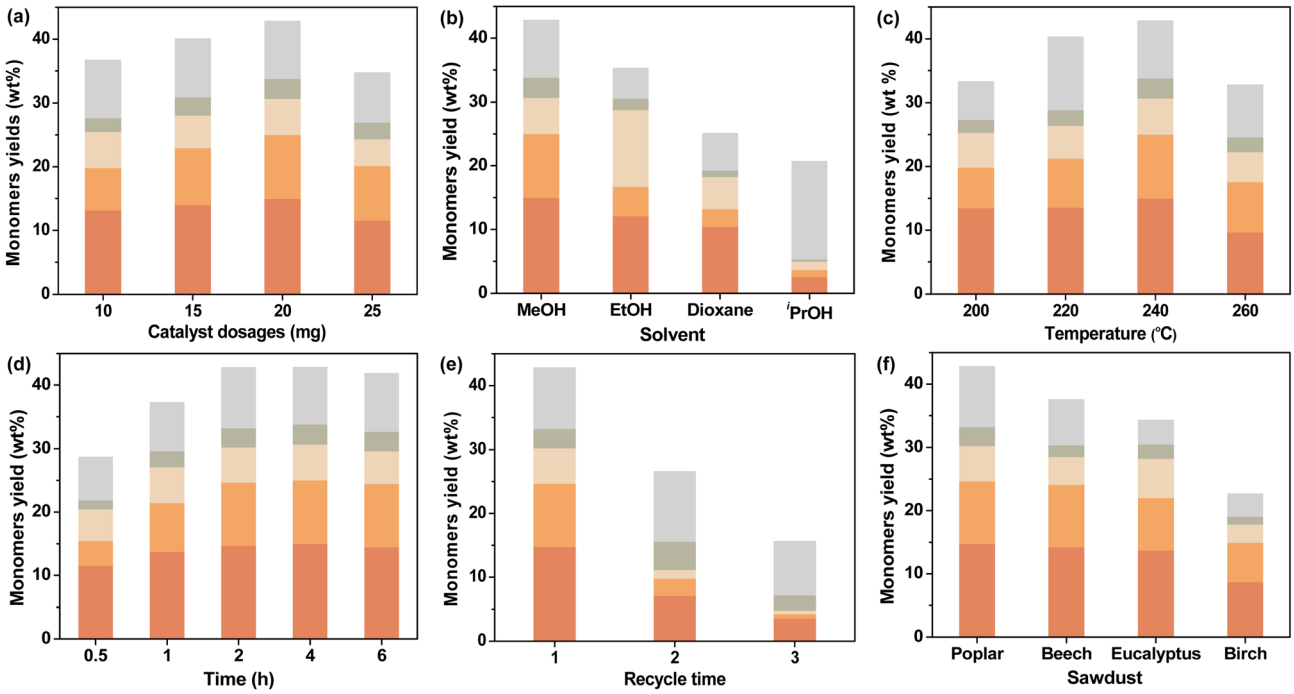

Fig. 5 Influences of (a) catalyst dosage, (b) solvent, (c) temperature and (d) time for RCD of poplar sawdust with CuO/c-UiO-66. (e) Stability of CuO/c-UiO-66. (f) Catalytic hydrogenolysis of various hardwood sawdust.

catalyst to escape through the pores of the screen. The separated catalyst was directly applied in the next cycle under the optimized reaction conditions. Notably, it was observed that the catalyst cycle could be performed three times with 15.7 wt% yield of monomers at the third cycle (Fig. 5e). The results of ICP analysis (Table S1†) and HADDF characterization (Fig. S4a†) of the spent catalyst showed a loss of copper species. We hypothesized that the decrease in catalytic activity could be due to the loss of the active center in the reducing hydrogen environment. Under such reaction conditions, the reactive center in the oxidation state might not be stably embedded in the MOF-derived support. Therefore, the next step is to design a Cu-based catalyst with more stable bonding between the active center and the carrier. However, to our delight, the fabricated CuO/c-UiO-66 revealed higher catalyst stability than our previously reported CuO/C.[56]

3.4 Hydrogenolysis of various hardwood sawdust

The hydrogenolysis of various hardwood samples, including beech, eucalyptus, and birch, was also performed over the CuO/c-UiO-66 catalyst under the optimized conditions to further evaluate the catalyst efficiency (Fig. 5f). Clearly, it was observed that all the three kinds of hardwoods afforded **S1** and **S2** as the main monophenols in high total yields (22.9–37.2 wt%). In a similar way to poplar sawdust, the RCD of other hardwood species underwent almost complete fragmentation of β-*O*-4′ linkages as illustrated by 2D HSQC NMR (Fig. S28–S30†). Suspiciously, it appeared that the copper-based catalysts were slightly less catalytically active on birch,[56] and the lower β-*O*-4′ content in birch may be one of the reasons for this, which will be further investigated in our laboratory. Notably, the distribution of monomers and GPC results are shown in Fig. S24 and S25,† which revealed a significant decrease of M_w of lignin oils after RCD of different hardwood sawdust in comparison with those of DELs. Low molecular weight aromatic monomers could be used to produce polymers with strong thermal stability by introducing reactive groups or molecules.[73–75] Furthermore, lignin monomers could be widely used in new products such as thermoplastics, coatings and resin materials.[75–78]

3.5 Mechanistic insights

In the blank control group, dimeric of β-*O*-4′ model compound **1** was reacted at 200 °C for 2 h (Fig. 6a). The generation of small amounts of 2-methoxy-4-(3-methoxy-1-propenyl)phenol **2** (34.7%) and **3** (32.4%) monomers was observed, as the hydrogen transfer reaction in supercritical MeOH could also achieve the cleavage of the C–O bonds, which is consistent with the blank experiments for depolymerizing poplar sawdust (Fig. 3a). For comparison, the above reaction proceeded in the presence of a combination of the CuO/c-UiO-66 catalyst and H_2. It gave 4-*n*-propanolguaiacol **G1** (9.8%), 4-*n*-propylguaiacol **G2** (30.0%), 4-ethylguaiacol **G3** (14.4%) and guaiacol **3** (55.5%) as the main products, which were derived from the hydrogenolysis of C_β–O linkages. The acidic and basic active sites on the surface of CuO/c-UiO-66 led to the acceleration of the hydrogen transfer process, which resulted in the efficient cleavage of the C–O bonds.

Compound **2** was not detected upon the addition of the catalyst as compared to the blank control group, so **2** might be an agent in the production of **G1** and **G2**.[35,79] In previous work,

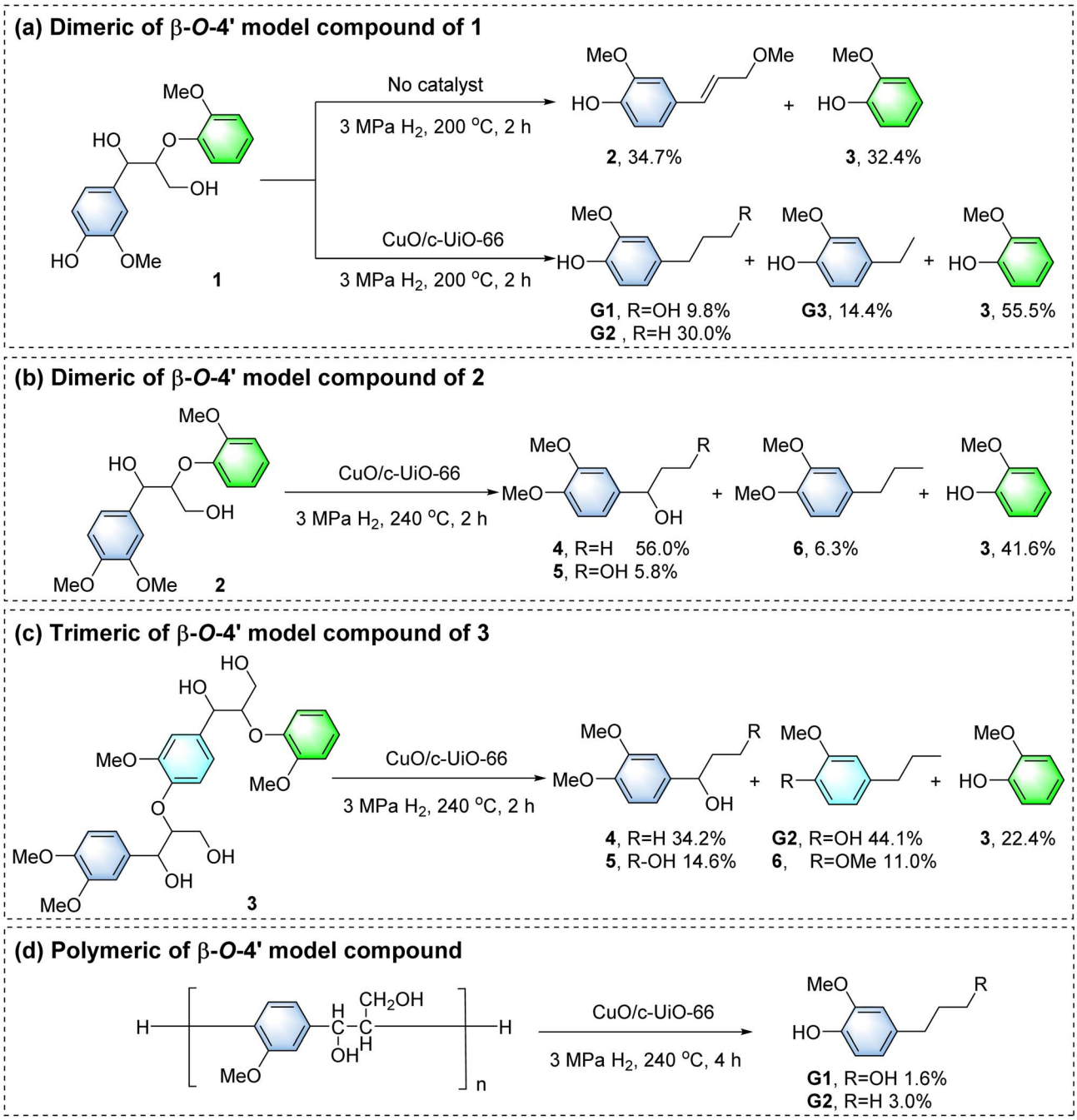

Fig. 6 Simulated reactivity of β-*O*-4′ lignin model compounds over the CuO/c-UiO-66 catalyst.

we confirmed that compound **2** was not generated *via* the reaction pathway of quinone radical products.[56] Therefore, in this catalytic system, the C_α–O and C_β–O bonds of the β-*O*-4′ molecule can be cleaved simultaneously. This provided important generative conditions for the production of **G1** and **G2**. **G1** almost completely reserved in the system (Fig. S37†), so the formation of **G1** may be due to the cleavage of C_α–O and C_β–O in the α-OMe β-*O*-4′ structure. The intermediate compound **2** undergoes a demethoxylation reaction to form **G2**.

The aromatic OMe groups played a key role in both oxidative polymerization and reductive depolymerization of lignin.[3,80,81] In order to exclude the effect of phenolic hydroxyl groups on the products, depolymerization of nonphenolic β-*O*-4′ dimer **2** has been proposed (Fig. 6b). It was found that the phenolic hydroxyl group prevented the elimination of the α-OH, and the C_γ–OH bond is probably split, forming 1-(3′,4′-dimethoxyphenyl)-1-propanol **4** (56.0%). In addition, 1-(3,4-dimethoxyphenyl) propane-1,3-diol **5** (5.8%), 1,2-dimethoxy-4-*n*-propylbenzene **6** (6.3%) and **3** (41.6%) were also generated. This result demonstrated that there was no hydromethylation of phenolic hydroxyl groups during the β-*O*-4′ alcoholysis. Otherwise, the α-OH would be retained. The depolymerization of trimer **3** with CuO/

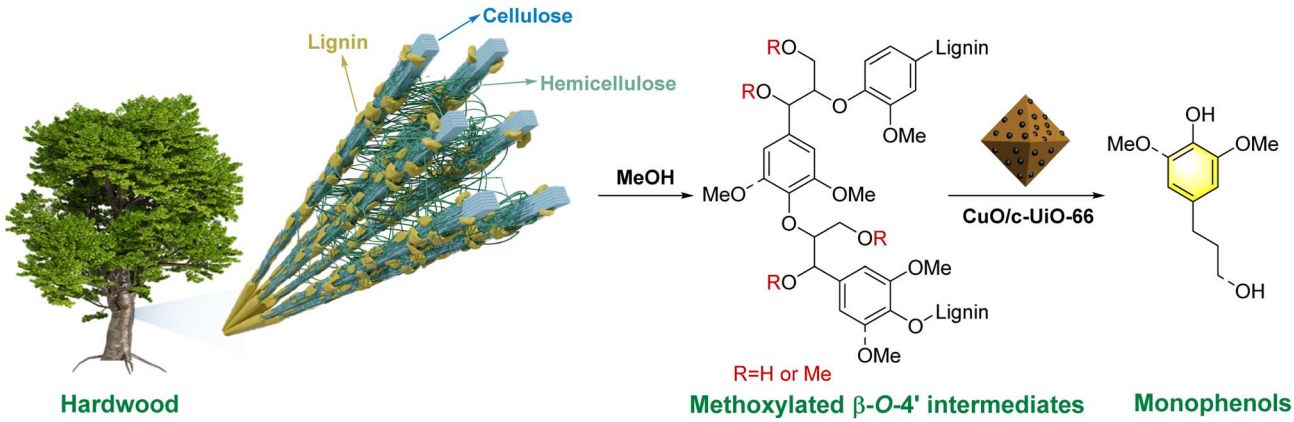

Fig. 7 Plausible reaction pathway for the reductive catalytic deconstruction of lignin from woody biomass into phenolic monomers over the CuO/c-UiO-66 catalyst.

c-UiO-66 also followed the same trend as the depolymerization of **2** (Fig. 6c). It should be noted that two C_β–O bond cleavages provided **4** (34.2%), **G2** (44.1%), **5** (14.6%), **3** (22.4%), and **6** (11.0%). Notably, **G1** was not detected, which could also be due to γ-OH methylation of trimer **3**.

To further simulate real lignin, the catalytic hydrogenation of β-*O*-4′ polymer was studied.[82] This polymer had been broken down to **G1** (1.6%) and **G2** (3.0%) (Fig. 6d), which was consistent with wood biomass. GPC analysis showed a remarkably lower M_w (700 g mol^{-1}) than β-*O*-4′ polymer (4190 g mol^{-1}) (Fig. S35†), demonstrating the successful depolymerization of the macromolecule. As reported, C-2 of the **G** unit reacted readily with C-5 in other lignin units, leading to the formation of condensed structures[83] and thus causing comparatively modest yields of the aromatic monomers.

Based on the mechanistic studies and relevant literature,[39,56,63] a plausible reaction pathway for the RCD of lignin from woody biomass into phenolic monomers over the CuO/c-UiO-66 catalyst is proposed in Fig. 7. In the natural biomass, nucleophilic substitution reactions might occur between MeOH and the β-*O*-4′ structure, resulting in α-OMe or α,γ-OMe. Subsequently, the synergistic effects of the catalyst and hydrogen lead to the efficient scission of the C–O bonds of the methoxylated β-*O*-4′ intermediates, affording the target monophenols.

4. Conclusions

We have reported a non-precious metal catalyst CuO/c-UiO-66 for the reductive hydrogenolysis of poplar lignin into monophenols in high yields (up to 42.8 wt%), which exhibited excellent catalytic properties. It was found that the CuO/c-UiO-66 showed satisfactory catalytic activity and good applicability in other hardwoods with high monomer yields (22.9–37.2 wt%). In view of the reactivity study of the β-*O*-4′ analogue, 4-propanol- and 4-propyl-substituted phenols could be formed directly over the CuO/c-UiO-66 catalyst. More specifically, it was also found that the two phenolic hydroxymethyl groups led to the retention of the α-OH group, which indicated that there was no methylation of the phenolic hydroxyl group under this catalytic system. The synergistic effect of the acid–base sites of the catalyst promoted the cleavage of the C–O bond. Of note was the optimum reactivity obtained under mild reaction conditions and the high catalytic rate of CuO/c-UiO-66. The next step is to further design a Cu-based catalyst with strong interactions between the active site and the substrate by our experimental platform for improving the cycling performance.

Conflicts of interest

There are no conflicts to declare.

Acknowledgements

This work was supported by the National Natural Science Foundation of China (22278049 and 51961125207), the Liaoning Revitalization Talents Program (XLYC2007104), and the Scientific Research Fund Program for Liaoning Provincial Department of Education (LJKZZ20220071).

References

1 Y. M. Questell-Santiago, M. V. Galkin, K. Barta and J. S. Luterbacher, *Nat. Rev. Chem.*, 2020, **4**, 311–330.
2 H. Li, A. Bunrit, N. Li and F. Wang, *Chem. Soc. Rev.*, 2020, **49**, 3748–3763.
3 Z. Liu, H. Li, X. Gao, X. Guo, S. Wang, Y. Fang and G. Song, *Nat. Commun.*, 2022, **13**, 4716.
4 S. Su, L.-P. Xiao, X. Chen, S. Wang, X.-H. Chen, Y. Guo and S.-R. Zhai, *ChemSusChem*, 2022, **15**, e202200365.
5 A. Avella, M. Ruda, C. Gioia, V. Sessini, T. Roulin, C. Carrick, J. Verendel and G. L. Re, *Chem. Eng. J.*, 2023, **463**, 142245.
6 M. Saidi, F. Samimi, D. Karimipourfard, T. Nimmanwudipong, B. C. Gates and M. R. Rahimpour, *Energy Environ. Sci.*, 2014, **7**, 103–129.
7 J. E. Holladay, J. F. White, J. J. Bozell and D. Johnson, *Top Value-Added Chemicals from Biomass – Volume II—Results of Screening for Potential Candidates from Biorefinery Lignin*, United States, 2007.

8 A. Bohre, A. Modak, V. Chourasia, P. R. Jadhao, K. Sharma and K. K. Pant, *Chem. Eng. J.*, 2022, **450**, 138032.
9 T. Nimmanwudipong, R. C. Runnebaum, D. E. Block and B. C. Gates, *Energy Fuels*, 2011, **25**, 3417–3427.
10 H. Luo, E. P. Weeda, M. Alherech, C. W. Anson, S. D. Karlen, Y. Cui, C. E. Foster and S. S. Stahl, *J. Am. Chem. Soc.*, 2021, **143**, 15462–15470.
11 Z. Sun, B. Fridrich, A. de Santi, S. Elangovan and K. Barta, *Chem. Rev.*, 2018, **118**, 614–678.
12 K. Barta, G. R. Warner, E. S. Beach and P. T. Anastas, *Green Chem.*, 2014, **16**, 191–196.
13 S. Constant, H. L. J. Wienk, A. E. Frissen, P. d. Peinder, R. Boelens, D. S. van Es, R. J. H. Grisel, B. M. Weckhuysen, W. J. J. Huijgen, R. J. A. Gosselink and P. C. A. Bruijnincx, *Green Chem.*, 2016, **18**, 2651–2665.
14 X. Huang, C. Atay, T. I. Korányi, M. D. Boot and E. J. M. Hensen, *ACS Catal.*, 2015, **5**, 7359–7370.
15 L.-P. Xiao, S. Wang, H. Li, Z. Li, Z.-J. Shi, L. Xiao, R.-C. Sun, Y. Fang and G. Song, *ACS Catal.*, 2017, **7**, 7535–7542.
16 R. C. Runnebaum, T. Nimmanwudipong, D. E. Block and B. C. Gates, *Catal. Sci. Technol.*, 2012, **2**, 113–118.
17 Y. Zhai, C. Li, G. Xu, Y. Ma, X. Liu and Y. Zhang, *Green Chem.*, 2017, **19**, 1895–1903.
18 Z. Sun, J. Cheng, D. Wang, T.-Q. Yuan, G. Song and K. Barta, *ChemSusChem*, 2020, **13**, 5199–5212.
19 M. M. Abu-Omar, K. Barta, G. T. Beckham, J. S. Luterbacher, J. Ralph, R. Rinaldi, Y. Román-Leshkov, J. S. M. Samec, B. F. Sels and F. Wang, *Energy Environ. Sci.*, 2021, **14**, 262–292.
20 D. Raikwar, K. Van Aelst, T. Vangeel, S. Corderi, J. Van Aelst, S. Van den Bosch, K. Servaes, K. Vanbroekhoven, K. Elst and B. F. Sels, *Chem. Eng. J.*, 2023, **461**, 141999.
21 R. M. O'Dea, P. A. Pranda, Y. Luo, A. Amitrano, E. O. Ebikade, E. R. Gottlieb, O. Ajao, M. Benali, D. G. Vlachos, M. Ierapetritou and T. H. Epps, *Sci. Adv.*, 2022, **8**, eabj7523.
22 L. Monsigny, E. Feghali, J.-C. Berthet and T. Cantat, *Green Chem.*, 2018, **20**, 1981–1986.
23 X. Liu, H. Li, L.-P. Xiao, R.-C. Sun and G. Song, *Green Chem.*, 2019, **21**, 1498–1504.
24 W. Schutyser, T. Renders, S. Van den Bosch, S. F. Koelewijn, G. T. Beckham and B. F. Sels, *Chem. Soc. Rev.*, 2018, **47**, 852–908.
25 J. Gracia-Vitoria, S. C. Gándara, E. Feghali, P. Ortiz, W. Eevers, K. S. Triantafyllidis and K. Vanbroekhoven, *Curr. Opin. Green Sustainable Chem.*, 2023, **40**, 100781.
26 K. Ye, Y. Liu, S. Wu and J. Zhuang, *Ind. Crop. Prod.*, 2021, **172**, 114008.
27 J. Zhang, *Green Energy Environ.*, 2018, **3**, 328–334.
28 J.-Y. Kim, J. Park, H. Hwang, J. K. Kim, I. K. Song and J. W. Choi, *J. Anal. Appl. Pyrol.*, 2015, **113**, 99–106.
29 T. Ren, S. You, Z. Zhang, Y. Wang, W. Qi, R. Su and Z. He, *Green Chem.*, 2021, **23**, 1648–1657.
30 F. Brienza, K. Van Aelst, F. Devred, D. Magnin, B. F. Sels, P. A. Gerin, I. Cybulska and D. P. Debecker, *ACS Sustainable Chem. Eng.*, 2022, **10**, 11130–11142.
31 K. Zhang, H. Li, L.-P. Xiao, B. Wang, R.-C. Sun and G. Song, *Bioresour. Technol.*, 2019, **285**, 121335.
32 R. Shu, Y. Xu, L. Ma, Q. Zhang, C. Wang and Y. Chen, *Chem. Eng. J.*, 2018, **338**, 457–464.
33 Y. Liao, S.-F. Koelewijn, G. Van den Bossche, J. Van Aelst, S. Van den Bosch, T. Renders, K. Navare, T. Nicolaï, K. Van Aelst, M. Maesen, H. Matsushima, M. T. Johan, K. Van Acker, B. Lagrain, D. Verboekend and F. Sels Bert, *Science*, 2020, **367**, 1385–1390.
34 X. Huang, O. M. M. Gonzalez, J. Zhu, T. I. Korányi, M. D. Boot and E. J. M. Hensen, *Green Chem.*, 2017, **19**, 175–187.
35 J. Hu, M. Zhao, B. Jiang, S. Wu and P. Lu, *Energy Fuels*, 2020, **34**, 9754–9762.
36 I. Nakamula, Y. Yamanoi, T. Imaoka, K. Yamamoto and H. Nishihara, *Angew. Chem., Int. Ed.*, 2011, **50**, 5830–5833.
37 Y. Wu, S. Cai, D. Wang, W. He and Y. Li, *J. Am. Chem. Soc.*, 2012, **134**, 8975–8981.
38 R. K. Sharma, S. Yadav, S. Dutta, H. B. Kale, I. R. Warkad, R. Zbořil, R. S. Varma and M. B. Gawande, *Chem. Soc. Rev.*, 2021, **50**, 11293–11380.
39 J. Sun, H. Li, L.-P. Xiao, X. Guo, Y. Fang, R.-C. Sun and G. Song, *ACS Sustainable Chem. Eng.*, 2019, **7**, 4666–4674.
40 S. Rautiainen, D. Di Francesco, S. N. Katea, G. Westin, D. N. Tungasmita and J. S. M. Samec, *ChemSusChem*, 2019, **12**, 404–408.
41 K. Barta, T. D. Matson, M. L. Fettig, S. L. Scott, A. V. Iretskii and P. C. Ford, *Green Chem.*, 2010, **12**, 1640–1647.
42 T. D. Matson, K. Barta, A. V. Iretskii and P. C. Ford, *J. Am. Chem. Soc.*, 2011, **133**, 14090–14097.
43 X. Huang, T. I. Korányi, M. D. Boot and E. J. M. Hensen, *ChemSusChem*, 2014, **7**, 2276–2288.
44 M. Chui, G. Metzker, C. M. Bernt, A. T. Tran, A. C. B. Burtoloso and P. C. Ford, *ACS Sustainable Chem. Eng.*, 2017, **5**, 3158–3169.
45 X. Zhu, Y. Liu, Y. Xiao, L. Zhong, T. Wang, Y. Wang and W.-P. Pan, *Chem. Eng. J.*, 2023, **467**, 143402.
46 C. Guo, F. Duan, S. Zhang, L. He, M. Wang, J. Chen, J. Zhang, Q. Jia, Z. Zhang and M. Du, *J. Mater. Chem. A*, 2022, **10**, 475–507.
47 D. Yang, V. Bernales, T. Islamoglu, O. K. Farha, J. T. Hupp, C. J. Cramer, L. Gagliardi and B. C. Gates, *J. Am. Chem. Soc.*, 2016, **138**, 15189–15196.
48 Y. Xue, S. Zheng, H. Xue and H. Pang, *J. Mater. Chem. A*, 2019, **7**, 7301–7327.
49 C.-Y. Fang, S. Zhang, Y. Hu, M. Vasiliu, J. E. Perez-Aguilar, E. T. Conley, D. A. Dixon, C.-Y. Chen and B. C. Gates, *ACS Catal.*, 2019, **9**, 3311–3321.
50 Q. Wang, Y. Tan, S. Tang, W. Liu, Y. Zhang, X. Xiong and Y. Lei, *ACS Nano*, 2023, **17**, 9565–9574.
51 Y. Wang, J. Wu, S. Tang, J. Yang, C. Ye, J. Chen, Y. Lei and D. Wang, *Angew. Chem., Int. Ed.*, 2023, **62**, e202219191.
52 C. He, J. Liang, Y.-H. Zou, J.-D. Yi, Y.-B. Huang and R. Cao, *Natl. Sci. Rev.*, 2022, **9**, nwab157.
53 J. Liang, R.-P. Chen, X.-Y. Wang, T.-T. Liu, X.-S. Wang, Y.-B. Huang and R. Cao, *Chem. Sci.*, 2017, **8**, 1570–1575.
54 Y.-H. Zou, Y.-B. Huang, D.-H. Si, Q. Yin, Q.-J. Wu, Z. Weng and R. Cao, *Angew. Chem., Int. Ed.*, 2021, **60**, 20915–20920.
55 Y.-L. Dong, Z.-Y. Jing, Q.-J. Wu, Z.-A. Chen, Y.-B. Huang and R. Cao, *J. Mater. Chem. A*, 2023, **11**, 8739–8746.

56 Q. Wang, L.-P. Xiao, Y.-H. Lv, W.-Z. Yin, C.-J. Hou and R.-C. Sun, *ACS Catal.*, 2022, **12**, 11899–11909.
57 T. Liu, X. Hong and G. Liu, *ACS Catal.*, 2020, **10**, 93–102.
58 W.-X. Li, W.-Z. Xiao, Y.-Q. Yang, Q. Wang, X. Chen, L.-P. Xiao and R.-C. Sun, *Ind. Crops Prod.*, 2021, **170**, 113692.
59 D. J. McClelland, A. H. Motagamwala, Y. Li, M. R. Rover, A. M. Wittrig, C. Wu, J. S. Buchanan, R. C. Brown, J. Ralph, J. A. Dumesic and G. W. Huber, *Green Chem.*, 2017, **19**, 1378–1389.
60 L. Li, J. Kong, H. Zhang, S. Liu, Q. Zeng, Y. Zhang, H. Ma, H. He, J. Long and X. Li, *Appl. Catal., B*, 2020, **279**, 119343.
61 Y. Wan, G. Yang, J. Xiang, X. Shen, D. Yang, Y. Chen, V. Rac, V. Rakic and X. Du, *Dalton Trans.*, 2020, **49**, 764–773.
62 F. Arena, G. Italiano, K. Barbera, S. Bordiga, G. Bonura, L. Spadaro and F. Frusteri, *Appl. Catal., A*, 2008, **350**, 16–23.
63 S. Van den Bosch, T. Renders, S. Kennis, S. F. Koelewijn, G. Van den Bossche, T. Vangeel, A. Deneyer, D. Depuydt, C. M. Courtin, J. M. Thevelein, W. Schutyser and B. F. Sels, *Green Chem.*, 2017, **19**, 3313–3326.
64 Z. Sun, G. Bottari, A. Afanasenko, M. C. A. Stuart, P. J. Deuss, B. Fridrich and K. Barta, *Nat. Catal.*, 2018, **1**, 82–92.
65 X. Gong, J. Sun, X. Xu, B. Wang, H. Li and F. Peng, *Bioresour. Technol.*, 2021, **333**, 124977.
66 S. Oh, S. Gu, J.-W. Choi, D. J. Suh, H. Lee, C. S. Kim, K. H. Kim, C.-J. Yoo, J. Choi and J.-M. Ha, *J. Environ. Chem. Eng.*, 2022, **10**, 108085.
67 M. Hou, H. Chen, Y. Li, H. Wang, L. Zhang and Y. Bi, *Energy Fuels*, 2022, **36**, 1929–1938.
68 S. Wang, K. Zhang, H. Li, L.-P. Xiao and G. Song, *Nat. Commun.*, 2021, **12**, 416.
69 S. Van den Bosch, W. Schutyser, R. Vanholme, T. Driessen, S. F. Koelewijn, T. Renders, B. De Meester, W. J. J. Huijgen, W. Dehaen, C. M. Courtin, B. Lagrain, W. Boerjan and B. F. Sels, *Energy Environ. Sci.*, 2015, **8**, 1748–1763.
70 L. Shuai, M. T. Amiri, Y. M. Questell-Santiago, F. Héroguel, Y. Li, H. Kim, R. Meilan, C. Chapple, J. Ralph and J. S. Luterbacher, *Science*, 2016, **354**, 329–333.
71 X. Ma, R. Ma, W. Hao, M. Chen, F. Yan, K. Cui, Y. Tian and Y. Li, *ACS Catal.*, 2015, **5**, 4803–4813.
72 Y. Deng, R. Gao, L. Lin, T. Liu, X.-D. Wen, S. Wang and D. Ma, *J. Am. Chem. Soc.*, 2018, **140**, 14481–14489.
73 A. L. Holmberg, J. F. Stanzione III, R. P. Wool and T. H. Epps III, *ACS Sustainable Chem. Eng.*, 2014, **2**, 569–573.
74 S. Wang, L. Shuai, B. Saha, D. G. Vlachos and T. H. Epps III, *ACS Cent. Sci.*, 2018, **4**, 701–708.
75 C. Gioia, G. Lo Re, M. Lawoko and L. Berglund, *J. Am. Chem. Soc.*, 2018, **140**, 4054–4061.
76 S. Wang, A. W. Bassett, G. V. Wieber, J. F. Stanzione III and T. H. Epps III, *ACS Macro Lett.*, 2017, **6**, 802–807.
77 S. Zhao and M. M. Abu-Omar, *Macromolecules*, 2017, **50**, 3573–3581.
78 W.-Z. Yin, L.-P. Xiao, Q. Wang, Y.-H. Lv, S.-L. Zou, Z. Wei and R.-C. Sun, *Composites, Part B*, 2023, **266**, 111013.
79 I. Kumaniaev, E. Subbotina, J. Sävmarker, M. Larhed, M. V. Galkin and J. S. M. Samec, *Green Chem.*, 2017, **19**, 5767–5771.
80 R. Vanholme, B. Demedts, K. Morreel, J. Ralph and W. Boerjan, *Plant Physiol.*, 2010, **153**, 895–905.
81 R. Rinaldi, R. Jastrzebski, M. T. Clough, J. Ralph, M. Kennema, P. C. A. Bruijnincx and B. M. Weckhuysen, *Angew. Chem., Int. Ed.*, 2016, **55**, 8164–8215.
82 C. S. Lancefield, O. S. Ojo, F. Tran and N. J. Westwood, *Angew. Chem., Int. Ed.*, 2015, **54**, 258–262.
83 X.-J. Shen, T. Chen, H.-M. Wang, Q. Mei, F. Yue, S. Sun, J.-L. Wen, T.-Q. Yuan and R.-C. Sun, *ACS Sustainable Chem. Eng.*, 2020, **8**, 2130–2137.

